HEAT TRANSFER STUDY OF 3-D PRINTED AIR-COOLED HEAT SINKS

Y.S. See* and K.C. Leong
*Author for correspondence
Singapore Centre for 3D Printing
School of Mechanical and Aerospace Engineering,
Nanyang Technological University,
50 Nanyang Avenue
Republic of Singapore,
E-mail: SEEY0017@e.ntu.edu.sg

ABSTRACT

The study explores the heat transfer capabilities of novel heat sinks fabricated by Selective Laser Melting (SLM), an additive manufacturing technique, subjected to an air jet impingement. Four different heat sinks were fabricated from AlSi10Mg powder and they consists of a cylindrical design, and three axially perforated designs, viz., hollow, tapered and nozzle. The results show that the Nusselt numbers of the cylindrical heat sink are up to 6.8% higher on average as compared to other heat sinks. However, the heat transfer for each unit cell for the cylindrical heat sink was worse than the other heat sinks, with the tapered heat sink being the best, performing an average of 84.6% better than the cylindrical heat sink. This is due to the increased surface area caused by perforations and the minimizing of air separation within the fins. The cylindrical heat sink was also compared with conventional fabricated heat sinks. It was found that the 3D printed cylindrical heat sink performs at a higher Nusselt number than the others at lower Reynolds number because of lower thermal resistances, but performs worse than the others at higher values due to the enhanced fluid mixing in the porous heat sinks.

INTRODUCTION

There has been an increasing drive to develop faster and cheaper computing devices while attempting to fabricate more miniature devices. However, the thermal management of such devices poses challenges that limit their capabilities [1]. The power dissipation has been increasing as technology advances. The increase is not linear but exponential and has been the trend for companies such as AMD Corporation and Intel Corporation as they strive to improve the microprocessors speeds [2]. One of the thermal management solutions introduced is impingement flow by air. Byon [3] suggested that jet impingement provided better cooling performance as compared to parallel flow and this concept was mainly used in the cooling of electronic components. El-Sheikh and Garimella [4] have also suggested that air jet impingement was capable of removing a similar amount of heat as compared to liquid cooling. Yang and Peng [5] suggested that air jet impingement methods had better unit price, weight and reliability as compared to other methods such as heat pipes. Jet impingement, combined with extended surfaces such as fins, have been considered to be one of the effective ways in dissipating heat. El-Sheikh and Garimella [4] showed in their study that finned heat sinks subjected to air impingement have a higher heat transfer coefficient than unfinned heat sinks. Maveety and Jung [6] conducted a comprehensive study on pin fin heat sinks subjected to air impingement such as the fin arrays, fin heights, nozzle placements, base thickness and effects of a deflector plate. In addition to fins, other researchers have explored the effects of perforations. Sahin and Demir [10] conducted a study of a single perforated pin fin configuration and showed that it performs better than solid fins. Ismail *et al.* [11] explored various shapes of perforations and determined that while solid fins may have higher Nusselt numbers compared to perforated fins, the heat removal rate is much lower than the perforated fins. Ismail *et al.* also determined that their circular perforated fins have the highest heat removal rate and perforated fin effectiveness among the other perforated shapes. In order to develop even more complex geometries for heat transfer enhancement, additive manufacturing is becoming a growing trend in fabricating various components including heat sinks [7, 12]. Selective Laser Melting (SLM), an additive manufacturing technique which is capable of fabricating metal parts of high density and good dimensional accuracy [8], can now be used to fabricate intricate heat sink designs.

The objective of this study is therefore to investigate the possibilities of using SLM to fabricate air-cooled heat sinks and to study their heat transfer performance under air jet impingement.

NOMENCLATURE

A	[m²]	surface area
B	[-]	scaling factor for Type 5 inclined manometer
D_h	[m]	hydraulic diameter
$\bar{h}$	[W/m²·K]	average heat transfer coefficient
k	[W/m·K]	thermal conductivity
m'	[kg]	mass of a single unit cell
N	[-]	number of unit cells
Nu	[-]	Nusselt number
p	[N/m²]	static pressure
$\dot{Q}$	[W]	heat transfer rate
Re	[-]	Reynolds number
T	[K]	temperature
v	[m/s]	velocity

Greek letters

ρ	[kg/m³]	density
μ	[kg/m·s]	dynamic viscosity

Subscripts

B	base of heat sink
HS	heat sink
in	input; from the transformer
losses	losses; heat losses from heat sink
nozzle	nozzle
∞	ambient

SELECTIVE LASER MELTING

One of the recent developments in manufacturing is Selective Laser Melting (SLM). It is a powder-based additive manufacturing technique in which a high powered laser beam is used to selectively melt powders in a powder bed. The laser melts only the surface of the powder bed, producing a single layer of the geometry required [8]. As the laser melts the powders, they fuse together to form a two-dimensional structure. The piston will then move a specific distance downwards and the recoating mechanism will re-supply another layer of powder. The process is repeated as more layers are melted in order to form the complete geometry. A schematic of SLM is presented in **Figure 1.** Such components can have almost 100% density [14]. The features of SLM therefore allow complex geometries to be fabricated.

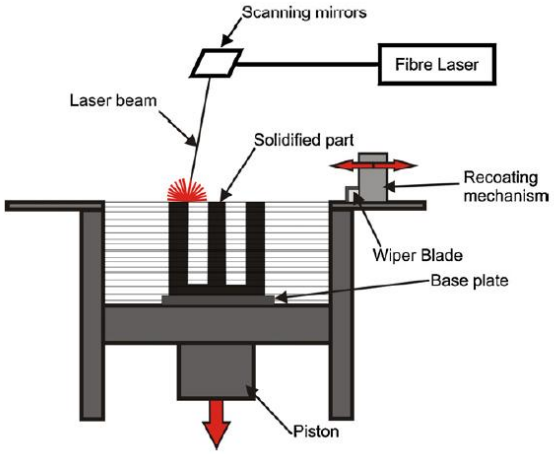

Figure 1 Schematic of SLM operating principle [17]

One of the major advantages of SLM compared to other additive manufacturing techniques is its ability to fabricate metallic components. Materials such as stainless steel, Inconel, titanium and aluminum alloys can be used with SLM [16]. The ability of SLM to fabricate metallic components provides opportunities to develop components primarily for heat transfer applications such as heat exchangers and heat sinks.

Aluminum alloys are preferred to stainless steel for heat sinks due to the former's higher thermal conductivity [16] which render them suitable for heat transfer applications. Thus, an aluminum alloy, AlSi10Mg, in powder form was used for fabricating the heat sinks in this paper.

DESIGN

In impingement, the air will not be able to penetrate towards the base of the heat sink due to the obstruction by the fins, causing a stagnation zone [9]. However, perforations in heat sinks have been found to remove more heat due to the extended surface area and minimized air separation from the fins [10, 11]. To take advantage of the perforations while minimizing the stagnation zone, heat sinks are designed as pin fin arrays with axial perforations. Three pin fin heat sinks were designed with axial perforations: the hollow pin fin, tapered pin fin and nozzle pin fin. A reference circular pin fin heat sink [12] was used for comparison. All heat sinks were fabricated using SLM with AlSi10Mg powder as the material. The overall design of each heat sink, together with the fin spacing and the overall base dimensions can be found in **Figure 2**.

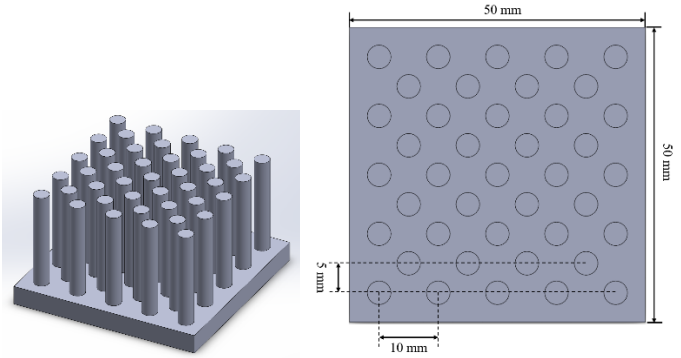

(a)

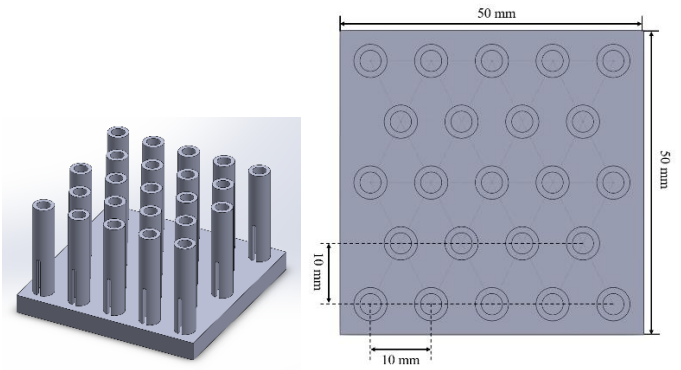

(b)

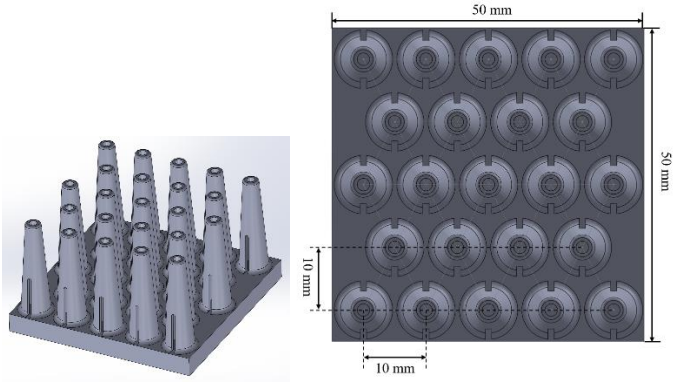

(c)

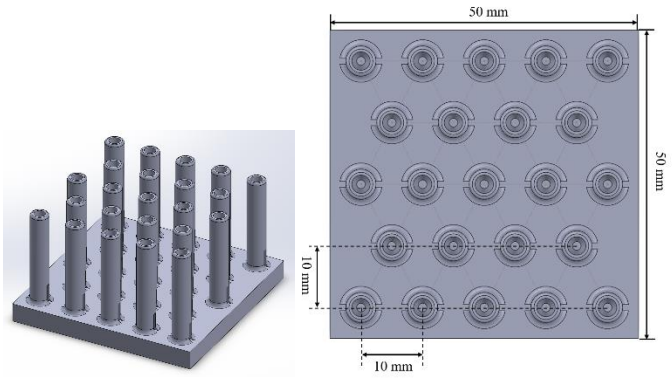

Figure 2 Four heat sinks. (a) The reference cylindrical heat sink [12], (b) hollow heat sink, (c) tapered heat sink and (d) nozzle heat sink

Each heat sink has a base of 50 mm by 50 mm and a thickness of 5 mm. All the fins on the heat sinks are of 25 mm height. Heat sinks with axial perforations have 23 fins each, while the reference cylindrical heat sink has 41 fins. The axial perforated heat sinks have two slits at the side of each fin with a height of 10 mm and width of 1 mm, except the nozzle heat sink with the slits measuring 5 mm height and 1 mm width. The slits provide passages for the air to flow out of the fins. **Figure 3** shows the dimensions for each fin and **Table 1** provides the details of the surface area, volume and mass of each heat sink.

EXPERIMENTAL SETUP AND PROCEDURES

The setup consists of two main parts: (1) the aluminum holder that houses the heaters and the heat sink and (2) the converging duct oriented in an impingement configuration. **Figure 4** shows a schematic of the experimental setup. The aluminum holder houses a Teflon block together with a 50 mm by 50 mm copper block where four cartridge heaters rated at 250 W each are inserted. The cartridge heaters were connected to a variable transformer. Each heat sink was bonded to the copper block with the OB-101 thermally conductive epoxy. Three K-type thermocouples were inserted into each heat sink to determine the average temperature of the heat sink. This is described in Figure 5. The converging duct has an inlet of 120 mm by 120 mm square and the outlet is a square nozzle of 10 mm by 10 mm. A "San Ace" 120 DC cooling fan was attached on top of the converging duct to provide an air flow towards the nozzle and to the heat sink. The fan is connected to a direct current power supply. A tripod supports the converging duct with the fan and sets it above the heat sink at a height of 6 mm. Four K-type thermocouples were positioned on the side and bottom walls of the aluminum housing to measure the temperatures necessary for heat loss calculation. One K-type thermocouple was used to measure the ambient temperature.

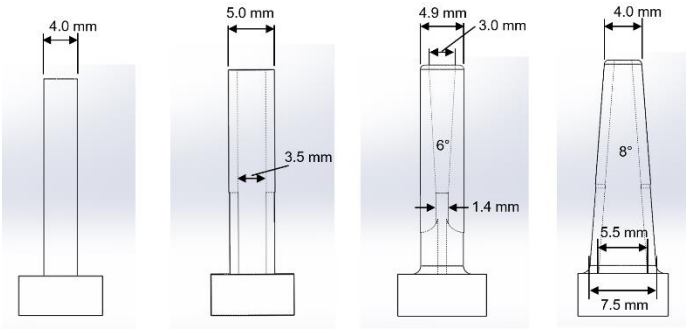

Figure 3 Dimensions of a single fin of each heat sink (a) cylindrical heat sink (b) hollow heat sink (c) nozzle heat sink (d) tapered heat sink

Table 1 Surface area, volume and mass of each heat sink

Heat Sink	Volume (mm^3)	Surface Area (mm^2)	Mass (g)
Cylindrical	25379.1	18880.3	54.6
Hollow	20146.6	22356.8	47.1
Tapered	20686.0	22837.6	47.5
Nozzle	21218.1	18548.5	50.6

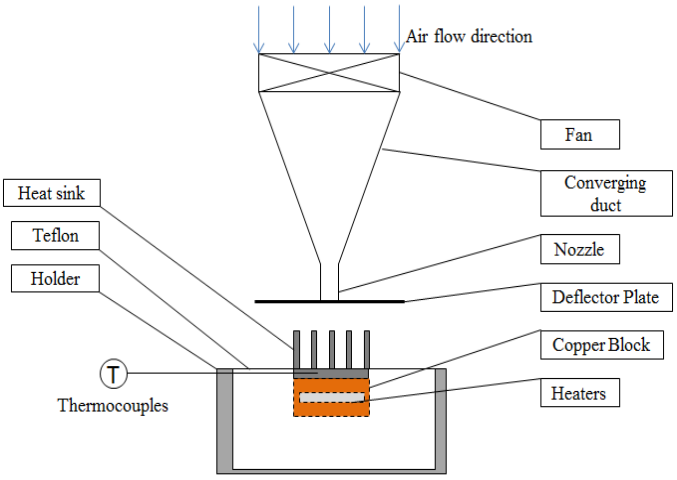

Figure 4 Schematic of experimental setup

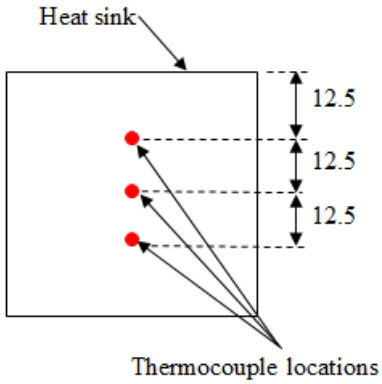

Figure 5 Positions of thermocouples within heat sink

Conduct of Experiments

Initial tests were conducted on the converging duct of the experiment facility to determine the Reynolds number for different power inputs to the fan. A pitot-static tube connected to a Type 5 inclined liquid manometer was positioned at the nozzle to measure the static pressure. The static pressure shown by the liquid manometer was used to calculate the velocities and subsequently the Reynolds number. Eight data points were obtained for the different air velocities by adjusting the power supply to the fan. The pitot-static tube was then removed and the power supply was set accordingly to achieve the desired velocity. Figure 6 provides the details of the static pressure against the power input. The velocities were determined to be between 6.1 m/s and 19.2 m/s based on the static pressure. Details on calculating the air velocities and therefore the Reynolds number are shown in the Mathematical Formulation section.

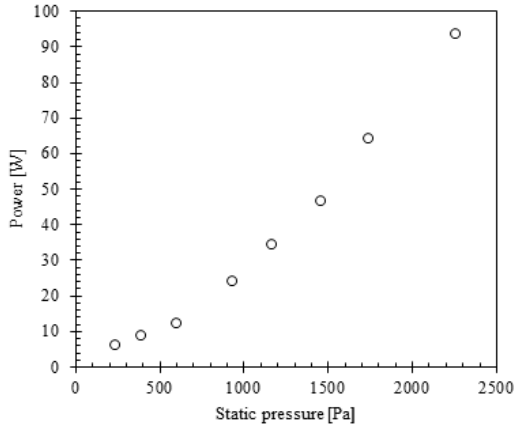

Figure 6 Power input to the fan against the static pressure

$\dot{Q}_{in}$ of 20 W was supplied by the cartridge heaters. The air velocity was set at the highest value (19.1 m/s) determined during the initial tests. The distance between the deflector plate and the tip of the heat sink was fixed at 6 mm, and the term 'nozzle height' is used to define this distance. Steady state condition was considered to be achieved when the temperature readings from the thermocouples fluctuated within ± 0.1°C for approximately 5 minutes and thereafter, the temperatures were recorded. At each velocity, steady state conditions were reached within approximately 30 minutes. The experiments were repeated for the other seven different velocities.

MATHEMATICAL FORMULATION

The Nusselt number is used to characterize the performance of each heat sink. The heat input to the heat sink, $\dot{Q}_{in}$ [W] is fixed at 20 W. This value is determined from the product of the voltage and current inputs as shown by the transformer. The heat losses, $\dot{Q}_{losses}$ are by natural convection from the aluminum holder on four sides and from the bottom surface. The correlations for natural convection based on the bottom surface and the vertical sides are given by Incropera *et al.* [13]. The range of Rayleigh numbers were determined to be between 4.2×10^5 and 8.4×10^5 for the four sides, and between 5.0×10^5 and 9.0×10^5 for the bottom surface. The calculated heat losses for the natural convection are therefore about 4.5% on average for all heat sinks. The radiation heat transfer rate is negligible due to the relatively small temperature difference between the base of the heat sink and the ambient temperature, ranging from 18.3°C to 31.4°C. The heat transfer rate to the heat sink is therefore

$$\dot{Q}_{HS} = \dot{Q}_{in} - \dot{Q}_{losses} \tag{1}$$

The average temperature of each heat sink is calculated from the three measured temperatures from the thermocouples as

$$T_{HS} = \frac{T_a + T_b + T_c}{3} \tag{2}$$

where T_a, T_b and T_c are the temperatures measured in the heat sink.

The average heat transfer coefficient is therefore calculated as

$$\bar{h}_{HS} = \frac{\dot{Q}_{HS}}{A_B\left(T_{HS} - T_\infty\right)} \tag{3}$$

where A_B is the heating surface of the heat sink, fixed at 250 mm², and T_∞ is the ambient temperature.

The Nusselt number is defined as

$$\mathrm{Nu} = \frac{\bar{h}_{HS} D_h}{k_{air}} \tag{4}$$

where k_{air} [W/m·K] is the thermal conductivity of air and D_h is the hydraulic diameter of the nozzle, and is fixed at 10 mm.

The air velocity v [m/s] is measured with a manometer and it can be defined

$$v = \sqrt{B \times \frac{2p}{\rho_{air}}} \tag{5}$$

where p is the static pressure measured from the liquid manometer, ρ_{air} [kg/m³] is the air density and B is the scale factor defined in the liquid manometer based on the inclination. Since only one inclination angle is used, a fixed value of B = 0.1 is defined.

The Reynolds number is defined

$$\mathrm{Re} = \frac{\rho_{air} v D_h}{\mu_{air}} \tag{6}$$

where μ_{air} [kg/m·s] is the dynamic viscosity of the air.

The properties of air are obtained based on the ambient temperature at 23°C, as the experiments were conducted at that temperature.

To investigate the effectiveness of the fin design, a parameter is introduced by the authors. The heat transfer rate per unit mass of unit cell is defined

$$\frac{\dot{Q}_{HS}}{Nm'} \tag{7}$$

Each unit cell is defined by a triangular boundary with the centers of the fin as the vertices. The unit cell consists of the half the fin and the base that is within the boundary. **Figure 7** shows the dimensions of the unit cell for each heat sink and **Table 2** shows the number of unit cells and the mass for each heat sink.

Table 2 Number of unit cell and the mass of each unit cell for various heat sinks

Heat Sink	No. of unit cells	Mass of unit cell (g)
Cylindrical	56	0.76
Hollow	28	1.12
Tapered	28	0.82
Nozzle	28	0.85

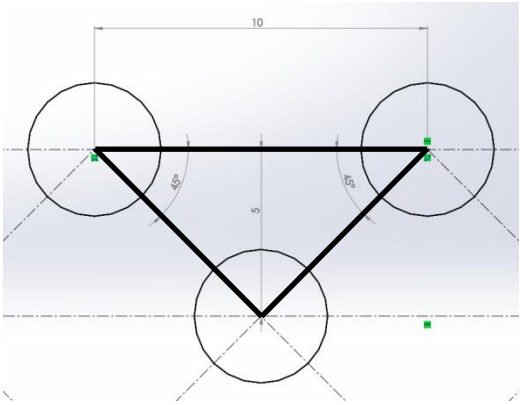

(a)

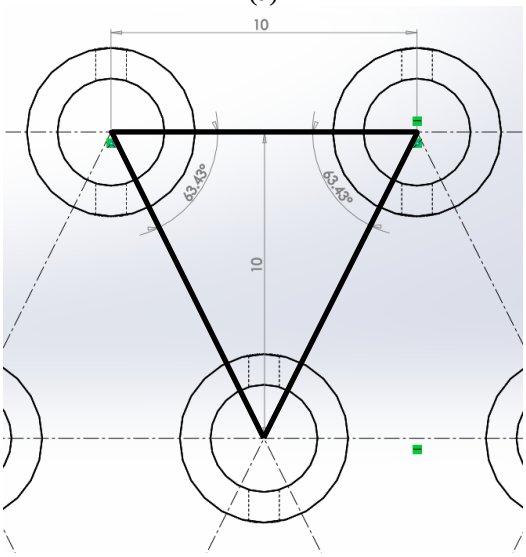

(b)

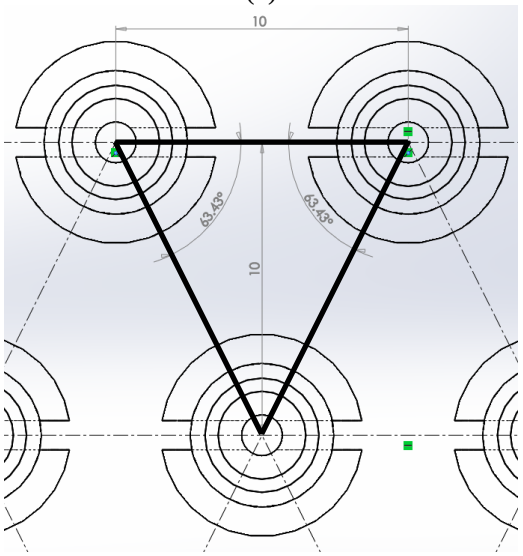

(c)

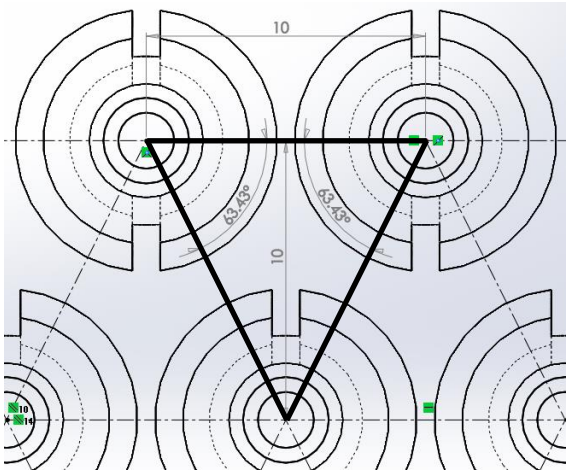

(d)

Figure 7 Unit cell dimensions for (a) cylindrical heat sink, (b) hollow heat sink (c) nozzle heat sink and (d) tapered heat sink. All heat sinks are viewed from plan view

The uncertainties of Nu and Re are determined using the method described by Moffat [18]. The general equations for the uncertainty for Nu and Re are defined as

$$\frac{\delta \mathrm{Nu}}{\mathrm{Nu}} = \sqrt{\left(\frac{\delta \bar{h}_{HS}}{\bar{h}_{HS}}\right)^2 + \left(\frac{\delta D_h}{D_h}\right)^2 + \left(\frac{\delta k_{air}}{k_{air}}\right)^2} \tag{8}$$

$$\frac{\delta \mathrm{Re}}{\mathrm{Re}} = \sqrt{\left(\frac{\delta \rho_{air}}{\rho_{air}}\right)^2 + \left(\frac{\delta \nu}{\nu}\right)^2 + \left(\frac{\delta D_h}{D_h}\right)^2 + \left(\frac{\delta \mu_{air}}{\mu_{air}}\right)^2} \tag{9}$$

The uncertainties of air properties are negligible and therefore are not considered in the above equations. The K-type thermocouples uncertainties are ±0.5°C for the experiments, and the temperature difference is between 18.3 °C and 31.4°C. The uncertainty of the transformer is ±1.9% for the power input. The uncertainty of the manometer is 1.4% for the static pressure, with the velocity ranging from 6.1 m/s to 19.2 m/s. The hydraulic diameter has an uncertainty of ±0.4%. The uncertainties for Nu and Re are on average ±3.0% and ±1.4%, with the maximum uncertainty of ±3.4% and ±4.4% respectively.

RESULTS AND DISCUSSION

Comparison among 3-D printed heat sinks

In **Figure 8,** comparisons of the Nusselt number against the Reynolds number for each heat sink are shown. It was found that the cylindrical heat sink has a higher Nu; on average 6.8%, 3.9%, and 4.9% higher than the hollow, tapered and nozzle heat sink respectively.

The governing factor for the improvement could possibly be the smaller cross-sectional area of the cylindrical heat sink which allows air to flow to the base at a higher velocity. The hollow, tapered and nozzle heat sinks have axial perforations and therefore larger cross-sectional areas, resulting in a lower air flow rate to the base as compared to the cylindrical heat sink. This phenomenon was also reported by Ismail *et al*. [11].

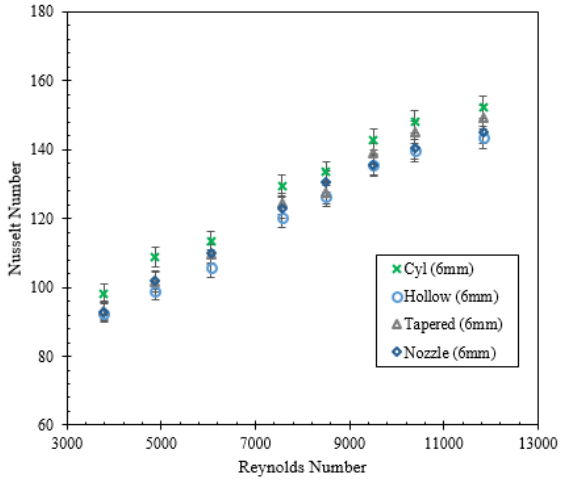

Figure 8 Nu of all heat sinks at various Re at nozzle height of 6 mm

Table 3 shows the heat transfer rate per unit mass of unit cell for each heat sink. It is found that the cylindrical heat sink has a lowest heat transfer performance per unit cell compared to the other heat sinks. The tapered heat sink performed best, followed by the nozzle, hollow and the cylindrical heat sink. The tapered heat sink has the highest heat transfer performance per unit cell on average approximately 37.6%, 2.7% and 84.6% better than the hollow, nozzle and cylindrical heat sinks, respectively. Based on the unit cell, the pin geometry of the tapered heat sink is the most effective in dissipating heat as compared to the others. The relatively larger external surface area as compared with the other heat sinks contributed to the higher heat dissipation per unit mass. Moreover, the internal surface area also provided additional surface for heat transfer. As shown by Ismail *et al*. [11] perforations in the heat sinks allow the air flowing through the perforation like a channel, thus reducing air separation from the fin, further enhancing heat transfer.

The nozzle pin geometry, despite having a much lower surface area also has similar heat transfer performances as compared to the tapered heat sink and was only approximately 2.7% lower. This is likely due to the acceleration of air within the perforation as it travels down the base, enhancing the heat transfer rate since the base of the heat sink receives a higher flow velocity, where dissipation of heat is more essential as was previously suggested by Sathe and Sammakia [9].

Table 3 Heat transfer performance per unit cell for each heat sink

Heat Sink	Heat transfer rate per unit mass of unit cell [W/kg]
Cylindrical	449.5
Hollow	603.0
Tapered	829.7
Nozzle	807.7

Comparison between 3-D printed heat sink and conventional heat sinks

A foam heat sink and a conventionally manufactured porous pin fin heat sink subjected to air impingement and described by Byon [3] are compared with the cylindrical heat sink presented in this paper. **Figure 9** shows the comparison between the three heat sinks. It can be seen that the 3-D printed cylindrical heat sink has a higher Nu than the two heat sinks at lower Re, but performs worse at higher Re, with the pin fin heat sink performing the best among the three. The better performance at low Re of the 3-D printed cylindrical heat sink may be attributed to the lower thermal resistance between the base and the fins as the heat sink was fabricated as a single entity. The poorer performance at higher Re may be due to the porosities of the foam and pin fin heat sinks that enhanced fluid mixing, which offsets their higher thermal resistance compared to the 3-D printed cylindrical heat sink.

However, further studies should be conducted to confirm such phenomenon.

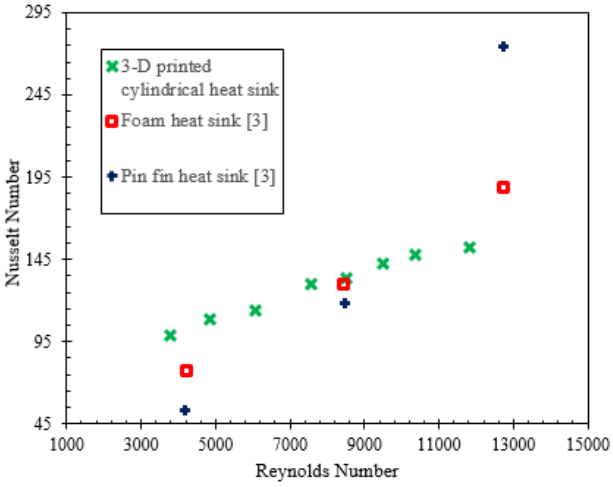

Figure 9 Comparison of 3-D printed cylindrical heat sink, foam heat sink [3], and conventionally manufactured pin fin heat sink described by Byon [3]

CONCLUSIONS AND RECOMMENDATIONS

Heat transfer studies of air cooled 3-D printed heat sinks with air jet impingement were conducted. The following conclusions can be drawn:

i. In terms of the Nusselt number, the cylindrical heat sink performed on average 6.8%, 3.9% and 4.9% better than the hollow, tapered and nozzle heat sink, respectively at 6 mm nozzle height. This is due to the smaller cross-sectional area for the air to flow, which increases its velocity and therefore the Nusselt number.

ii. The tapered heat sink has the highest heat transfer performance per unit cell, approximately 37.6%, 2.7% and 84.6% better than the hollow, nozzle and cylindrical heat sink respectively at 6 mm nozzle height. The larger cross-sectional area of axially perforated heat sinks, together with lower air separation experienced within the perforations, enhances the heat transfer rate.

iii. The 3-D printed heat sinks perform better at lower Re compared with conventionally manufactured heat sinks, but worse at higher Re. The lower thermal resistance of the 3-D printed heat sink may have contributed to the improvement.

Additive manufacturing enables heat sinks of complex pin geometries to be fabricated. The complexity may enhance the heat transfer performance, opening up opportunities to the development of novel heat sink designs for air impingement. Further studies could be performed on the air pressure drop of the heat sinks and visualization of the air flow to investigate the fluid dynamics within each heat sink experimentally. Such a study can determine the effectiveness of axial perforations and the drag force experimentally. Other further studies can include exploration of various fin shapes other than the circular shape. More robust investigations should also be conducted to compare between additive manufactured and conventionally produced heat sinks for approximately the same thermal conductivities and masses.

ACKNOWLEDGMENT

Funding for the SLM facility by the National Research Foundation, Singapore, is gratefully acknowledged.

REFERENCES

[1] Moore, A.L. and Li, S., Emerging challenges and materials for thermal management of electronics, *Materials Today*, Vol. 17, No. 4, 2014, pp. 163 – 174.

[2] Azar, K. (2000, Jan 1). *The history of power dissipation* [Online]. Available: http://www.electronics-cooling.com/2000/01/the-history-of-power-dissipation/ , Retrieved on 26 Feb 2016.

[3] Byon, C., Heat transfer characteristics of aluminum foam heat sinks subject to an impinging jet under fixed pumping power, *International Journal of Heat and Mass Transfer*, Vol. 85, 2015, pp. 1056 – 1060.

[4] El-Sheikh, H.A. and Garimella, S.V., Enhancement of air jet impingement heat transfer using pin-fin heat sinks, *IEEE Transactions*

on Components and Packaging Technologies, Vol. 23, No. 2, 2000, pp. 300 – 308.
[5] Yang, Y.-T. and Peng, H.-S., Numerical study of pin-fin heat sink with un-uniform fin height design, *International Journal of Heat and Mass Transfer*, Vol. 51, 2008, pp. 4788 – 4796.
[6] Maveety, J.G. and Jung, H. H., Heat transfer from square pin-fin heat sinks using air impingement cooling, *IEEE Transactions on Components and Packaging Technologies*, Vol. 25, No. 3, 2002, pp. 459 – 469.
[7] Wong, M., Owen, I., Sutcliffe, C.J. and Puri, A., Convective heat transfer and pressure losses across novel heat sinks fabricated by selective laser melting, *International Journal of Heat and Mass Transfer*, Vol. 52, 2009, pp. 281 – 288.
[8] Chua, C.K. and Leong, K.F., 3*D Printing and Additive Manufacturing: Principles and Applications*, 4th ed., World Scientific Publishing, pp. 264 – 265.
[9] Sathe, S.B. and Sammakia, B.G., An analytical study of the optimized performance of an impingement heat sink, *Transactions of the ASME*, Vol. 126, 2004, pp. 528 – 534.
[10] Sahin, B. and Demir, A., Performance analysis of a heat exchanger having perforated square fins, *Applied Thermal Engineering*, Vol. 28, 2008, pp. 621 – 632.
[11] Ismail, M.F., Hasan, M.N. and Ali, M., Numerical simulation of turbulent heat transfer from perforated plate-fin heat sinks, *Heat and Mass Transfer*, Vol. 50, 2014, pp. 509 – 519.
[12] Ho, J.Y., Wong, K.K., Leong, K.C. and Wong, T.N., Convective heat transfer performance of airfoil heat sinks fabricated by selective laser melting, *International Journal of Thermal Sciences*, Vol. 114, 2017, pp. 213 – 228.
[13] Incropera F.P., DeWitt D.P., Bergman T.L. and Lavine A.S. *Principles of Heat and Mass Transfer*. 7th ed. John Wiley & Sons; 2013.
[14] Wong, K.K., Ho, J.Y., Leong, K.C. and Wong, T.N., Fabrication of heat sinks by Selective Laser Melting for convective heat transfer applications, *Virtual and Rapid Prototyping*, Vol. 11, 2016, pp. 159 – 165.
[15] Abe, F., Osakada, K., Shiomi, M., Uematsu, K., Matsumoto, M., The manufacturing of hard tools from metallic powders by selective laser melting. *Journal of Materials Processing Technology*, Vol. 111, Issue 1 – 3, 2001, pp. 210 – 213.
[16] Wong, M., Tsopanos, S., Sutcliffe, C.J., Owen, I., Selective laser melting of heat transfer devices. *Rapid Prototyping Journal*, Vol. 13, Issue 5, 2007, pp. 291 – 297.
[17] Louvis, E., Fox, P., Sutcliffe, C.J., Selective laser melting of aluminium components, *Journal of Materials Processing Technology*, Vol. 211, 2011, pp. 275 – 284. Available: https://www.researchgate.net/publication/251609729_Selective_laser_melting_of_aluminium_components
[18] Moffat, R.J., Using uncertainty analysis in the planning of an experiment, *Journal of Fluids Engineering*, Vol. 107, 1985, pp. 173 – 178.